scientific reports

OPEN

Metamaterial conical beam antenna with dual band filtering response

Xianfeng Tang[1]✉, Junli Lu[1,2], Xiangqiang Li[1,2], Che Xu[1]✉, Qingfeng Wang[1,2] & Jianqiong Zhang[1,2]

A novel conical beam antenna with dual band filtering response is proposed by utilizing a metamaterial (MTM). The dual band filtering characteristics are inherently derived from the MTM and achieved through the coaxial feed and the probe coupling. Meanwhile, the conical beam is realized by using the cylindrical probe within the antenna aperture. Notably, the antenna exhibits remarkable compactness: firstly, the transverse size of the MTM is only ~ $\lambda_1/7$ or ~ $\lambda_2/5$, where λ_1 and λ_2 are the free space wavelength of central frequencies of the MTM's two modes, respectively. Secondly, extra filters are circumvented owing to the filtering performance of the MTM. To substantiate the aforementioned characteristics, the proposed MTM antenna is designed, fabricated, and measured. The measured results show a good agreement with the simulated ones, indicating that the proposed conical beam antenna has two operating bands around 3 GHz and 4.3 GHz, respectively. Additionally, the excellent filtering performance is confirmed by the out-of-band gain suppression level of ~ 30 dB outside the two passbands. It is feasible to use the MTM to develop the dual band filtering antenna with conical radiation.

Keywords Filtering antenna, Metamaterial, Dual band, Conical radiation

Recently, conical beam antennas have attracted much attention to target tracking, local-area network, ground satellite communication terminals, and other areas due to the ability to produce a specific radiation pattern with omnidirectional radiation in azimuth and a null in zenith[1–3]. At present, there are several approaches to construct conical beam antennas. Typically, open-ended coaxial waveguides excited by TEM mode could be used to produce the conical beam[4,5]. Z. Shen, et al. demonstrated that a top-hat monopole is an excellent candidate for generating conical beam[6]. H. Nakano, et al. proposed the spiral conical beam antenna by utilizing a two-arm round spiral structure[7]. In[8,9], the conical beam antenna is constructed by the slotted circular waveguide with one short-circuited terminal. Furthermore, the conical beam can also be achieved through array antennas[10,11], or planar antennas with distinct radiation patches[12–14].

In order to contribute to system miniaturization as well as improve system performance, numerous attempts have been undertaken to incorporate extra functionalities[15–20] such as high gain, frequency configurability, circularly polarized antenna, fixed linear and circular polarization into conical beam antennas. To achieve the dual-band operation for conical beam antennas, one approach involves the utilization of nested horn antennas[21], while another approach relies on the dual-mode cross-slotted cylindrical waveguides[22]. Furthermore, to simultaneously achieve the dual-band operation and filtering response, one can introduce the extra filter into the nested horn antenna[23]. While this approach effectively ensures dual-band filtering capability, it does increase the complexity of the conical beam antennas.

Metamaterials (MTMs), which refer to artificial composite subwavelength structures, have been extensively used in designing antennas[24,25]. For example, Li et al. proposed a novel miniaturized magnetoelectric dipole antenna by using the magnetic metamaterial[26]. Rajanna, et al. introduced the zero-index metamaterial into microstrip patch antenna for gain enhancement[27]. Li et al. achieved the bow-tie antenna with high gain and miniaturization based on artificial magnetic conductor and MTM lens[28]. Additionally, MTMs can also be utilized to improve bandwidth[29], reduce the radar cross section of antennas[30], enhance the isolation in multiple-input–multiple-output antennas[31], and achieve dual band antennas[32].

Here, leveraging the metamaterial (MTM)[33], we present a novel approach for constructing conical beam antennas that exhibit dual band operation, filtering response, and miniaturization. The dual band operation is

[1]School of Physical Science and Technology, Southwest Jiaotong University (SWJTU), Chengdu 611756, China. [2]Junli Lu, Xiangqiang Li, Qingfeng Wang and Jianqiong Zhang contributed equally to this work. ✉email: txf_2012@163.com; xuche@swjtu.edu.cn

derived from the two modes of only one kind of MTM, avoiding the utilization of two different MTMs. Also, the filtering performance originates from the inherent stopband of the MTM, thus eliminating extra filters. Moreover, the MTM demonstrates compactness as its transverse size is significantly smaller than that of a hollow waveguide at the same frequencies.

Methods
Characteristics of the MTM
As we know, the hollow square waveguide with the transverse sizes of 14.5 mm × 14.5 mm, as shown in Fig. 1a, has a cut-off frequency of ~ 10.34 GHz according to the waveguide theory[34]. Commonly, when the filled dielectric of air keeps unchanged, the transverse sizes must be enlarged to reduce the cut-off frequency. For example, the square hollow waveguide such as WR-284 waveguide operating at 2.6–3.95 GHz has the transverse sizes of 72.14 mm × 34.04 mm.

Here, a complementary electric split ring resonator (CeSRR) shown in Fig. 1b is inserted into the center of the hollow square waveguide to form the MTM[33], as shown in Fig. 1c. The dispersion curves of the MTM are obtained by using the eigenmode solver in HFSS[35], as shown in Fig. 1d. As we see, the MTM exhibits two distinct modes with central frequencies of approximately $f_1 = 3$ GHz and $f_2 = 4.3$ GHz, respectively. The two distinct modes correspond to two separate passbands, providing the precondition to the dual band operation. The inherent stopbands outside the two operating frequency bands can provide the filtering response. According to the effective medium theory, the CeSRR can be characterized by the effective permittivity tensor[33]

$$\bar{\bar{\varepsilon}} = \varepsilon_0 \begin{bmatrix} \varepsilon_{xx} & 0 & 0 \\ 0 & 1 & 0 \\ 0 & 0 & \varepsilon_{zz} \end{bmatrix} \tag{1}$$

The empty square waveguide, which can be considered as a one-dimensional magnetic plasma for TM-mode[36–38], offers the effective permeability $\mu = \mu_0 \mu_{eff} = \mu_0 \left(1 - f_c^2/f^2\right)$. Here, ε_0 and μ_0 are the permittivity and the

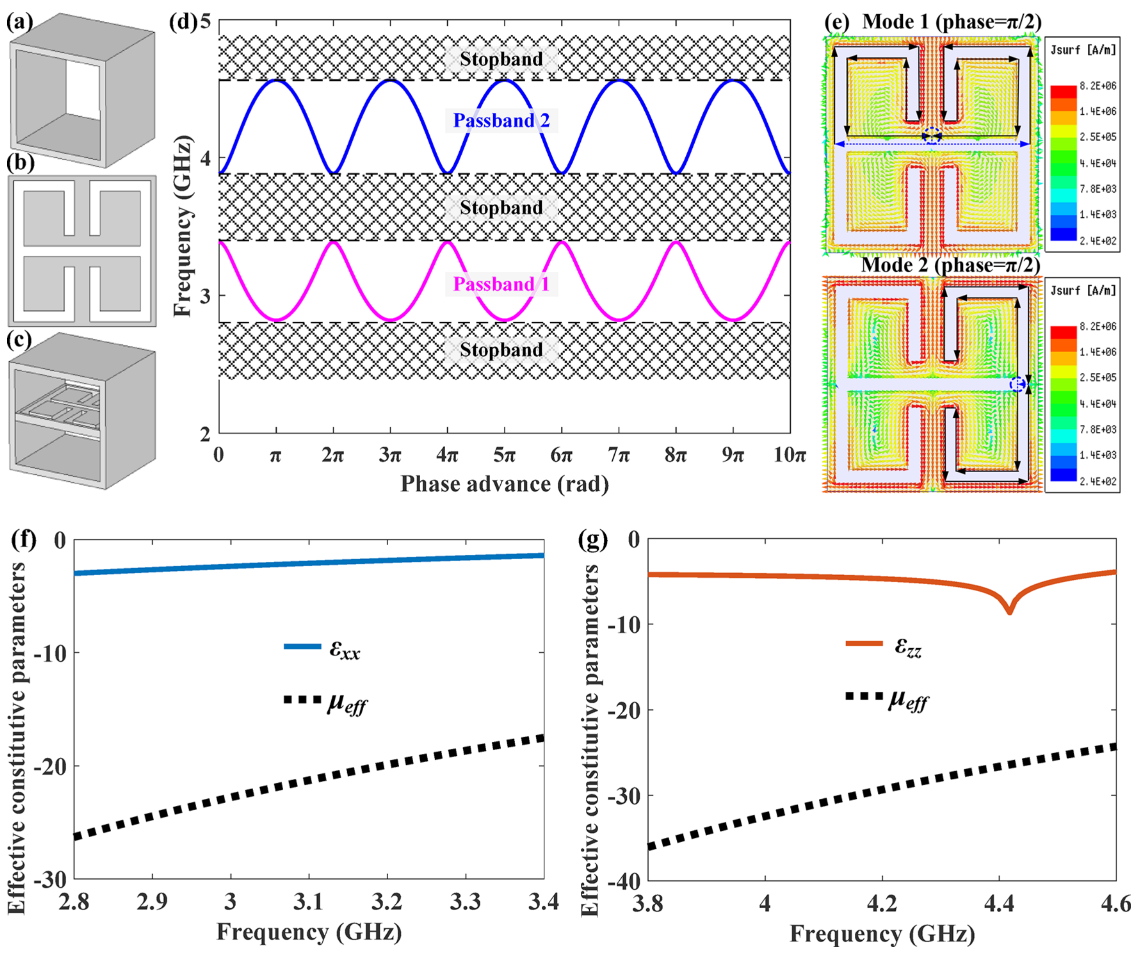

Fig. 1. (**a**) Hollow square waveguide, (**b**) CeSRR, (**c**) MTM unit cell, (**d**) dispersion curves for two modes of the MTM, (**e**) surface current distribution for two modes on the CeSRR, effective constitutive parameters for (**f**) mode 1 and (**g**) mode 2.

permeability in vacuum, respectively, ε_{zz} and ε_{xx} are the relative permittivity parameters, μ_{eff} is the relative permeability, f is the operating frequency, and f_c is the cutoff frequency. As a result, the obtained effective constitutive parameters are shown in Fig. 1f,g. The MTM exhibits left-handed characteristics in the two frequency bands corresponding to the two modes, in which CeSRRs offer negative effective permittivity and the empty square waveguide operating below the cut-off frequency offers the negative effective permeability[38].

Furthermore, the surface current distribution of the two modes on the CeSRR is shown in Fig. 1e. According to the method in Ref.[39], the resonant frequency of the CeSRR f_s can be calculated by $f_s = c_0/l_{cir}$, where c_0 and l_{cir} are the speed of light in the vacuum and the circumference of the inner wall of the long slot-line, respectively. As a result, the CeSRR has two resonant frequencies of ~3.33 GHz and ~4.55 GHz, corresponding to the Lorentz-like response frequencies of the two distinct modes[33]. The resonant characteristics of the CeSRR offer the foundation for the MTM operating below the cutoff frequency of the hollow square waveguide. As a result, we can enlarge or decrease l_{cir} by adjusting the parameters of the MTM and thus the operating frequency bands of the MTM antenna would be correspondingly changed. As a comparison, the MTM has the similar operating frequency with the WR-284 waveguide, but the former has less than one-tenth cross sectional area of the latter. The results clearly indicate that the MTM exhibits the advantage of miniaturization. The MTM offers a novel approach to the realization of the miniaturized antenna with multifunctionalities including the dual band operation and the filtering capability.

Design of the MTM antenna

As shown in Fig. 2a, the proposed MTM antenna includes three parts, that is, an MTM, a coaxial feed, and a square aperture. The MTM with eight unit cells offers the dual band operation of the antenna due to its two distinct modes, as shown in Fig. 2b. The two ends of the MTM are connected by the coaxial feed and the square aperture, respectively. The former facilitates the propagation of the electromagnetic wave from the coaxial line into the MTM, while the latter guarantees its radiation from the MTM into the free space.

The coaxial feed consists of the standard Sub Miniature version A (SMA), the matched block, and the first CeSRR with two blended edges, as shown in Fig. 2c. The SMA is used to feed the proposed antenna and its inner conductor is directly inserted into the CeSRR. As shown in Fig. 2d, the matched block is integrated onto the first CeSRR and aligned precisely with its center. This matched block between the SMA and the MTM is beneficial for the impedance matching. Meanwhile, the two edges of the first CeSRR should be blended to enhance the match at the second operating passband[40].

At the terminus of the antenna, the last CeSRR, the square aperture and the cylindrical probe together constitute the transition between the MTM and the free space. Here, part of the last CeSRR is inserted into the square aperture and a cylindrical probe is extended from the end of the CeSRRs, as shown in Fig. 2e. The radiation characteristics of the proposed antenna are determined by the square aperture as well as the cylindrical probe. The square aperture radiating the electromagnetic wave from the MTM into the free space can be considered as the open-ended waveguide. Meanwhile, the cylindrical probe within the square aperture contributes to the formation of the conical beam.

The antenna match in the MTM's two operating passbands depends on both the coaxial feed and the square aperture with the cylindrical probe. Here we analyze the effect of the square aperture parameters on the

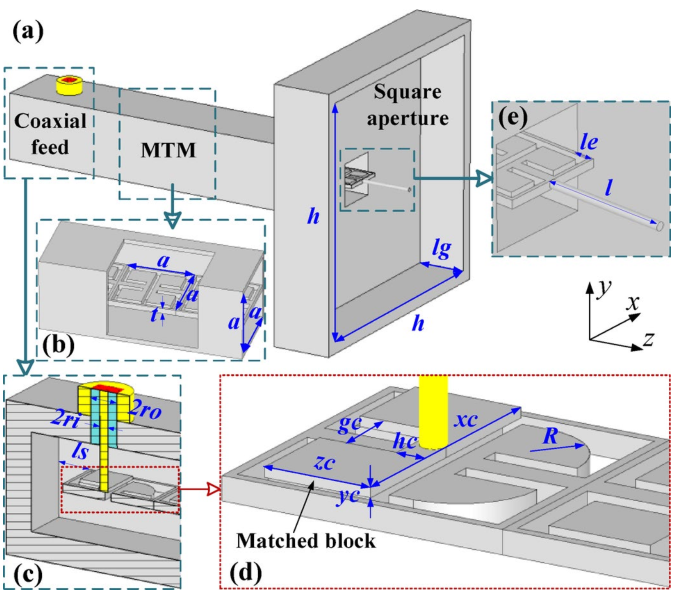

Fig. 2. Configuration of the proposed MTM antenna. (**a**) Overall perspective view of the antenna, (**b**) side view of the MTM, (**c**) side view of the coaxial feed, (**d**) zoomed-in section of first CeSRR and the matched block, (**e**) zoomed-in section of the last CeSRR and the cylindrical probe in the square aperture.

reflection coefficient $|S_{11}|$ of the proposed antenna by using CST Microwave Studio[41]. The corresponding results are presented in Fig. 3.

Figure 3a shows $|S_{11}|$ for different probe length l. It is clear that the absence of the cylindrical probe significantly improves $|S_{11}|$. Meanwhile, the antenna exhibits a mismatch when $l = 25$ mm which approximates to the quarter-wavelength in free space at 3 GHz. The results highlight the significant distinction between the probe coupling in the proposed antenna and the monopole antenna. As is known, the length of the monopole antenna is associated with the wavelength or the operating frequency. Figure 3b shows $|S_{11}|$ for different le. As we see, it is beneficial for improving the match by inserting the last CeSRR into the square aperture though $|S_{11}|$ is not sensitive to le. Figure 3c,d show $|S_{11}|$ for different lg and h. The results indicate that the square aperture as the open-ended waveguide is crucial for enhancing the impedance match at the two operating bands.

The proposed antenna has a radiation mechanism that combines the open-ended waveguide and the monopole antenna. On one hand, the transition between the MTM and the free space, that is the square aperture within the cylindrical probe, shares some structural similarities with the open-ended waveguide. Meanwhile, the two operated modes in the MTM are TM-dominated modes, as shown in Fig. 4. Hence, it can be regarded as a novel open-ended waveguide excited by the TM-dominated mode. On the other hand, the proposed antenna exhibits part of the radiation characteristics of the common monopole antenna, that is the conical beam. The difference is that the monopole antenna operates within a single band[6] and the operating frequency is dependent on its length. While the cylindrical probe in the proposed antenna is used to ensure the good match at both of the two operating bands and is not directly correlated with the frequency. Furthermore, the TEM electromagnetic wave in the coaxial line would be transformed to TM-dominated mode in the MTM. Then, the TM-dominated wave would be selectively radiated into the free space due to the MTM's dual band operation. Meanwhile, TM-dominated wave would be transformed to the TEM one in the free space. Here, the coaxial feed and the transition serve dual roles as the mode converter as well as the impedance transformer.

Based on the aforementioned analysis, we have obtained the optimized parameters of the proposed MTM antenna, as listed in Table 1. It is worth mentioning that other detail parameters of the MTM unit cell can be found in Ref. 38. Consequently, the reflection coefficient $|S_{11}|$, realized gain, efficiency, and the 3D far field radiation patterns are shown in Fig. 5. It is clear that the antenna exhibits two operating bands with 260 MHz and 330 MHz, corresponding to the two passbands of the MTM shown in Fig. 1. Typically, the realized gains are 2.69 dBi, 2.83 dBi, 4.6 dBi and 4.54 dBi at 2.95 GHz, 3 GHz, 4.3 GHz, and 4.35 GHz, respectively. The

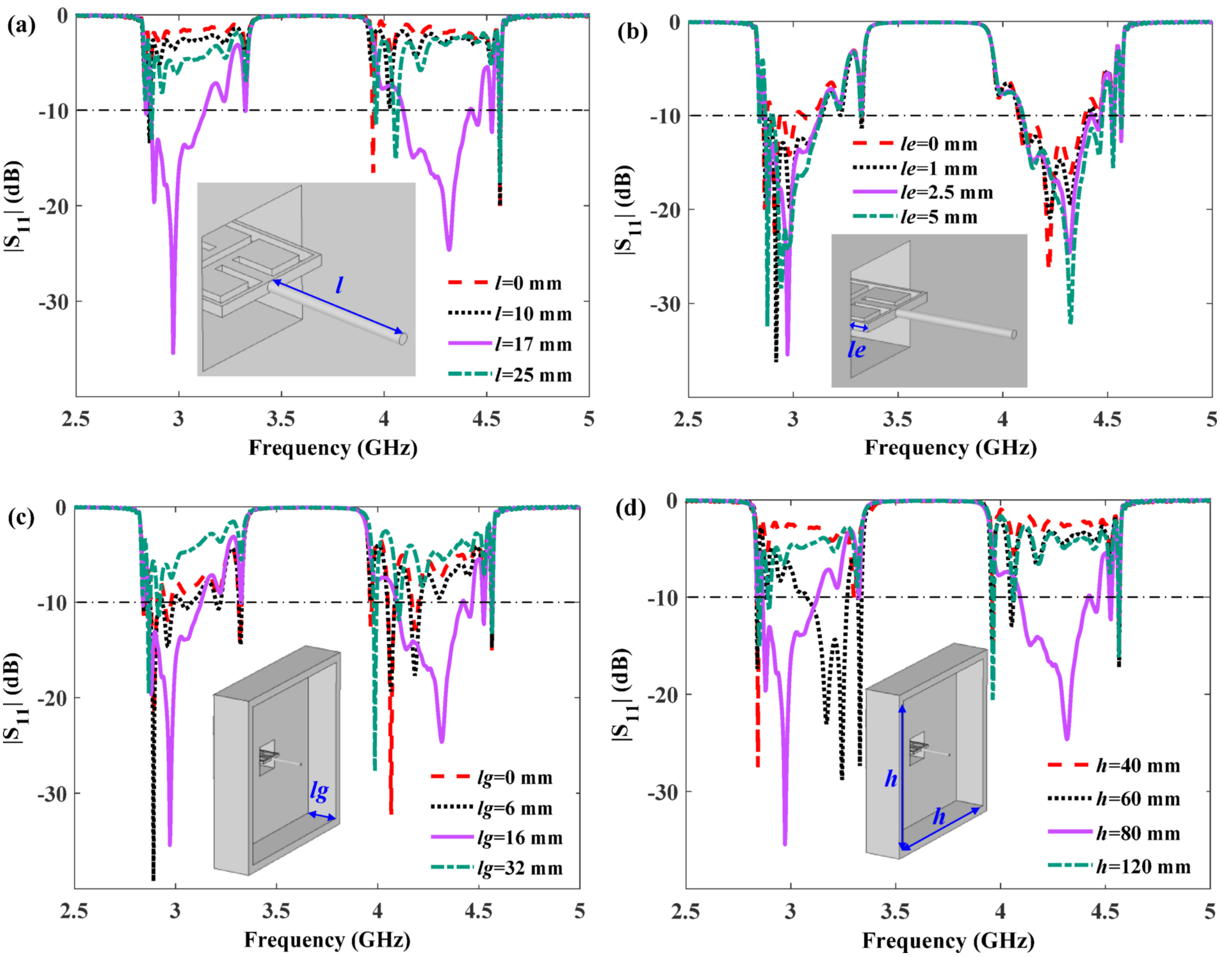

Fig. 3. $|S_{11}|$ for (**a**) different l, (**b**) different le, (**c**) different lg, and (**d**) different h.

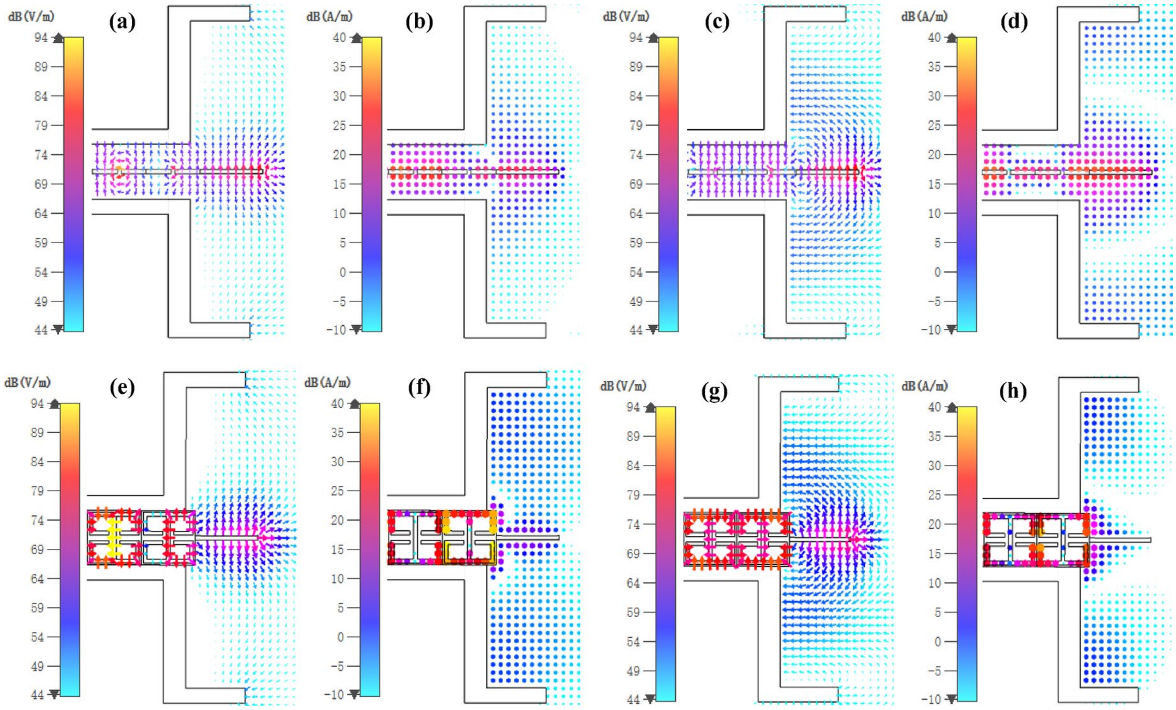

Fig. 4. (**a**) Electric field and (**b**) magnetic field distribution at 3 GHz in *yoz* plane, (**c**) electric field and (**d**) magnetic field distribution at 4.3 GHz in *yoz* plane, (**e**) Electric field and (**f**) magnetic field distribution at 3 GHz in *xoz* plane, (**g**) electric field and (**h**) magnetic field distribution at 4.3 GHz in *xoz* plane.

Parameter	Value (mm)	Parameter	Value (mm)	Parameter	Value (mm)
a	14.5	*h*	80	*le*	2.5
t	1.2	*hc*	1.5	*lg*	16
zc	5.5	*xc*	13	*ls*	5
yc	0.5	*gc*	3.5	*l*	17
ri	0.65	*ro*	2.1	*R*	4

Table 1. Optimized parameters of the MTM antenna.

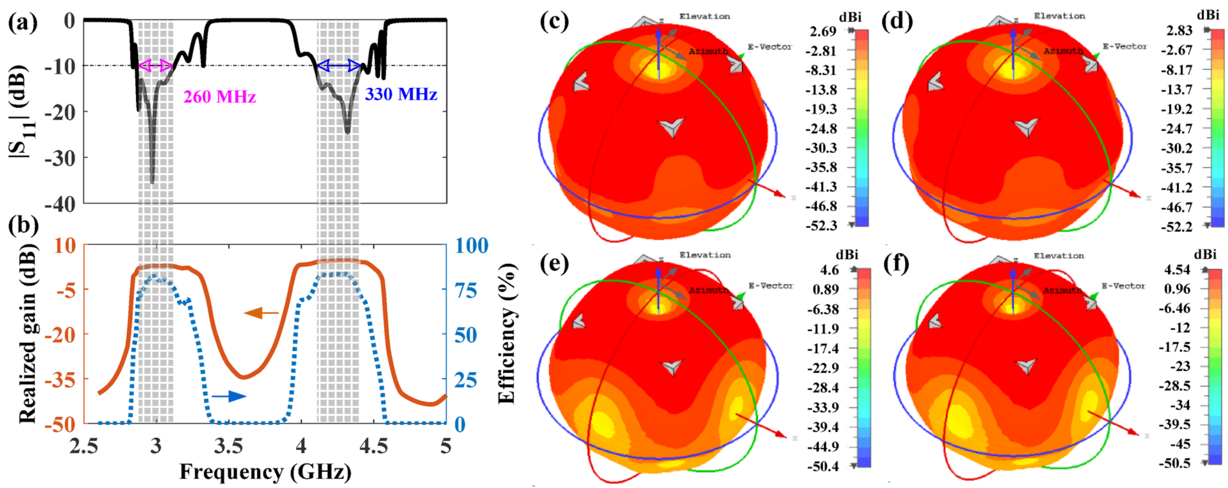

Fig. 5. (**a**) Optimized $|S_{11}|$, (**b**) realized gain and efficiency, 3D far field radiation patterns at (**c**) 2.95 GHz, (**d**) 3 GHz, (**e**) 4.3 GHz, and (**f**) 4.35 GHz.

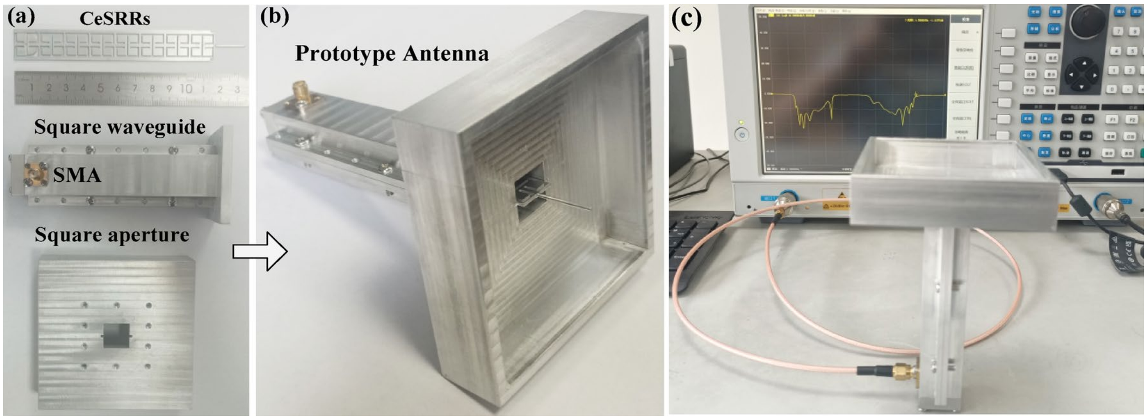

Fig. 6. (**a**) Fabricated components, (**b**) prototype antenna, and (**c**) reflection experiment set.

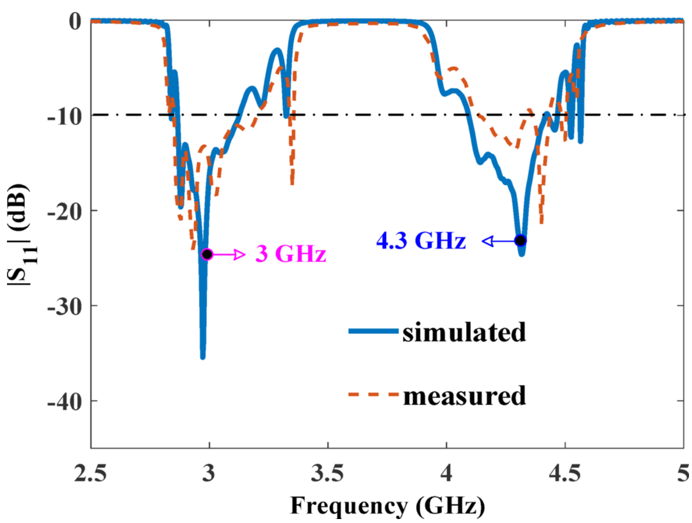

Fig. 7. Measured $|S_{11}|$ with respect to the simulated one.

maximum efficiencies at the two operating bands are ~ 83%. The realized gains at the two passbands are not symmetrical due to the following reasons. First, the two modes have different theoretical bandwidth as shown in Fig. 1d. Second, the strongest reflection null in the first passband is closer to the lower cutoff frequency of mode 1 and the one in the second passband is closer to the upper cutoff frequency of mode 2, as shown in Fig. 5a. This is because the two modes share the common structure but have different electric field distribution, as shown in Fig. 4. Third, the sizes of the antenna relative to the wavelength are also different for the two modes. Furthermore, as we see from Fig. 5c–f, the obvious nulls in zenith of the patterns confirm the conical radiation characteristics of the MTM antenna.

Results
Reflection measurement of the MTM antenna
We have fabricated the prototype antenna to measure its predicted performance. The components of the MTM antenna are displayed in Fig. 6a, consisting of the SMA, the square waveguide, the CeSRRs with the matched block and the cylindrical probe, and the square aperture. The SMA filled with Teflon has a 50 Ω impedance. The matched block and the cylindrical probe are integrated on the CeSRRs. The square waveguide is fabricated to two split parts for being easily inserted into the CeSRRs. The SMA receptacle is mounted on the matched block of the MTM to construct the coaxial feed. The antenna assembly is completed by fixing the square aperture on the other end of the MTM. The completed antenna assembly is shown in Fig. 6b. Here, low-speed wire electrical discharge machining with a fabrication tolerance of 0.005 mm is utilized to fabricate the CeSRRs with the matched block and the cylindrical probe, and the antenna material is aluminum with conductivity 2.3×10^7 S/m.

A vector network analyzer has been utilized to measure $|S_{11}|$ of the prototype antenna, as shown in Fig. 6c. The measured $|S_{11}|$ as well as the simulated one is plotted in Fig. 7. The measured results align well with the simulated ones, affirming that the proposed antenna exhibits two passbands, approximately at 3 GHz and 4.3 GHz

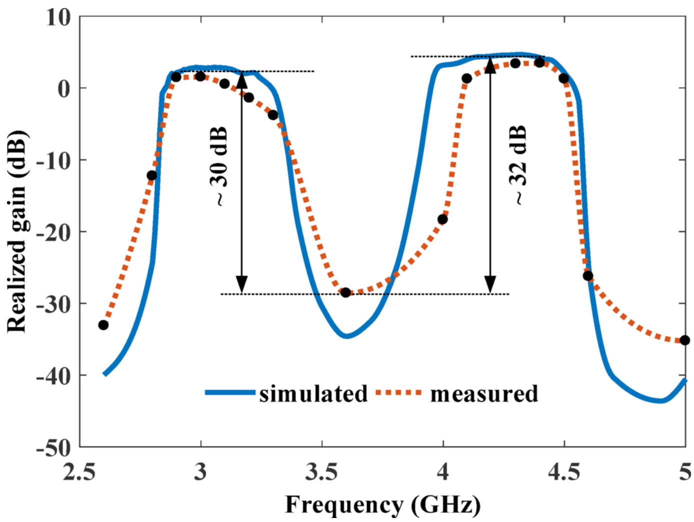

Fig. 8. The measured and simulated realized gain.

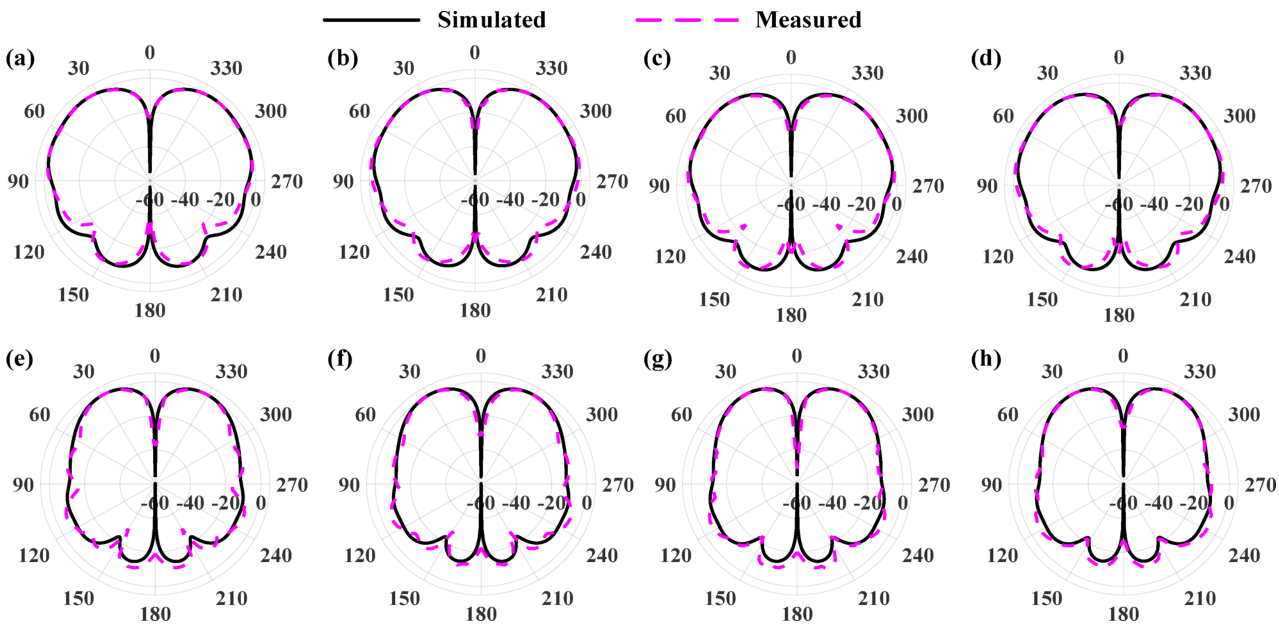

Fig. 9. Normalized radiation patterns for 2.95 GHz (**a**) at xoz plane and (**b**) at yoz plane, for 3 GHz (c) at xoz plane and (**d**) at yoz plane, for 4.3 GHz (**e**) at xoz plane and (**f**) at yoz plane, for 4.35 GHz (**g**) at xoz plane and (**h**) at yoz plane.

respectively. While it should be noted that slight discrepancies exist between the measured and simulated results, which is derived from fabrication tolerances.

Measurement of the far field radiation patterns

Two standard horn antennas are utilized to measure the realized gains and far field radiation patterns of the prototype antenna in a microwave anechoic chamber. One is a 15-dB standard gain horn antenna ranging from 2.6 to 3.95 GHz and the other is a 10-dB standard gain horn antenna ranging from 3.9 to 6 GHz. Figure 8 shows the comparison between the simulated and measured realized gains. It is clear that the measured realized gains align well with the simulated ones though there is a little difference between them for inevitable machining and measured errors. Furthermore, the realized gain sharply decreases outside the operating frequency bands. The antenna demonstrates the out-of-band gain suppression level (OBGSL) of approximately 30 dB and 32 dB with respect to the gains at the first and second operating frequency bands, respectively. The facts confirm the excellent filtering response of the proposed dual band antenna using the MTM.

Furthermore, the measured and simulated far field radiation patterns for 2.95 GHz, 3 GHz, 4.3 GHz, and 4.35 GHz are shown in Fig. 9a–h, respectively. As we see, the measured results closely match the simulated ones.

Refs	[21]	[22]	[23]	[42]	This work
Antenna type	Horn	Waveguide	Horn	Planar	MTM
Dual band operation	Yes	Yes	Yes	Yes	Yes
Filtering response	No	No	Yes	Yes	Yes
Conical beam	Yes	Yes	Yes	No	Yes
Central freq. (GHz)	10/35	28/38.5	24.7/33.8	3.45/5	3/4.3
OBGSL (dB)	N/A	N/A	No data	18.1/17.7	30/32
Null depth (dB)	− 25 to − 30*	− 25 to − 30*	− 18 to − 30*	N/A	− 22 to − 50
Volume (λ_1^3)	1.7 × 1.7 × 1*	0.7 × 0.7 × 24.5**	2.78 × 2.45 × 3.03	0.75 × 0.75 × 0.13	0.8 × 0.8 × 1.4
Volume (λ_2^3)	6 × 6 × 3.5**	1 × 1 × 33**	3.8 × 3.4 × 4.1**	1.1 × 1.1 × 0.18**	1.15 × 1.15 × 2
Gain (dBi)	9.2/11.6	14.5/14.2	8.8/6.4	8.5/9	2.8/4.5
Efficiency (%)	N/A	83–90	> 83	> 90	~ 83

Table 2. Comparison of the proposed antennas and reference antennas. λ_1 represents the wavelength corresponding to the lower operating frequency band. λ_2 represents the wavelength corresponding to the higher operating frequency band. *Read from figures. **Estimated from the data in the table.

The main beam directs at approximately ± 41 degrees at frequencies 2.95 GHz and 3 GHz, and ± 29 degrees at frequencies 4.3 GHz and 4.35 GHz. Additionally, the beam gain at 0 degree is much smaller than that at the main beam directions, indicating a null depth from − 22 dB to − 50 dB. These observations confirm that the proposed MTM antenna exhibits the conical radiation at two frequency bands.

Discussion

A comparison between this work and the reference antennas is presented in Table 2. The proposed antenna exhibits the following merits. Firstly, the proposed antenna eliminates extra filters while demonstrates remarkable filtering response with the OBGSL of approximately 30 dB. Secondly, the null depth of − 22 to − 50 dB confirms the outstanding conical radiation characteristics. Thirdly, with respect to the current conical beam antennas, this work has lower gain mainly due to two reasons. On one hand, the radiating element is the monopole. On the other hand, the effective aperture area of the antenna is limited by small transverse sizes of the MTM. Hence, the proposed antenna achieves the miniaturization advantage and dual band filtering response from the MTM and thus sacrifices the gain. In the future, we will explore methods to enhance the gain of this antenna, such as using arrays, among others.

In this paper, an MTM conical beam antenna with the dual-band filtering response is reported. The reflection experiments reveal the low reflection characteristics for the proposed antenna around the frequencies of 3 and 4.3 GHz respectively and thus verify the dual band operation. While the gain measurements demonstrate that the antenna has good filtering response outside the above two passbands. Furthermore, the conical radiation with a null depth of − 22 dB to − 50 dB, achieved by the probe coupling within the antenna aperture, is confirmed by the far field radiation pattern measurements. The work presents a novel approach for constructing conical beam antennas that exhibit dual band operation, filtering response, and miniaturization.

Data availability

The data that support the findings of this study are available from the corresponding authors upon reasonable request.

Received: 4 July 2024; Accepted: 18 April 2025
Published online: 04 May 2025

References

1. Gao, Y. et al. A dual-polarized 2-D monopulse antenna array for conical conformal applications. *IEEE Trans. Antennas Propag.* **69**, 5479–5488. https://doi.org/10.1109/TAP.2021.3060085 (2021).
2. Gao, Y. et al. A dual-polarized 2-D monopulse antenna array for conical conformal applications. *IEEE Trans. Antennas Propag.* **69**(9), 5479–5488. https://doi.org/10.1109/TAP.2021.3060085 (2021).
3. MahdiTaskhiri, M. & Fakhte, S. Broadband inhomogeneous lens with conical radiation pattern. *Sci. Rep.* **13**, 12907. https://doi.org/10.1038/s41598-023-40024-9 (2023).
4. Qi, S., Wu, W., Fang, D. G. & Shen, Z. Circular aperture antenna with conical beam. *IEEE Antennas Wirel. Propag. Lett.* **10**, 211–214. https://doi.org/10.1109/LAWP.2011.2128297 (2011).
5. Shen, Z., Wang, J. & Lee, K. S. Open-ended coaxial waveguide for conical-beam radiation. *IEEE Trans. Antennas Propag.* **60**(5), 2518–2521. https://doi.org/10.1109/TAP.2012.2189720 (2012).
6. Shen, Z. & Wang, J. Top-hat monopole antenna for conical-beam radiation. *IEEE Antennas Wireless Propag. Lett.* **10**, 396–398. https://doi.org/10.1109/LAWP.2011.2152359 (2011).
7. Nakano, H., Oyanagi, H. & Yamauchi, J. A wideband circularly polarized conical beam from a two-arm spiral antenna excited in phase. *IEEE Trans. Antennas Propag.* **59**(10), 3518–3525. https://doi.org/10.1109/TAP.2011.2163759 (2011).
8. Liu, Y. et al. Leaky-wave antenna with switchable omnidirectional conical radiation via polarization handedness. *IEEE Trans. Antennas Propag.* **68**(3), 1282–1288. https://doi.org/10.1109/TAP.2019.2927865 (2020).

9. Sanchez-Olivares, P., Masa-Campos, J. L., Garcia-Marin, E. & Escalona-Moreno, D. High-gain conical-beam traveling-wave array antenna based on a slotted circular waveguide at Ku-Band. *IEEE Trans. Antennas Propag.* **68**, 6435–6440. https://doi.org/10.1109/TAP.2020.2970031 (2020).
10. Cao, Y. F., Zhang, X. Y. & Mo, T. Low-profile conical-pattern slot antenna with wideband performance using artificial magnetic conductors. *IEEE Trans. Antennas Propag.* **66**(5), 2210–2218. https://doi.org/10.1109/TAP.2018.2809619 (2018).
11. Hua, D., Qi, S. S., Wu, W. & Fang, D. G. CPW-fed printed antenna array with conical beam. *IEEE Trans. Antennas Propag.* **64**, 1096–1100. https://doi.org/10.1109/TAP.2015.2513087 (2016).
12. Guo, Y. X., Chia, M. Y. W., Cheng, Z. N. & Luk, K. M. Wide-band L-probe fed circular patch antenna for conical-pattern radiation. *IEEE Trans. Antennas Propag.* **52**(4), 1115–1116. https://doi.org/10.1109/TAP.2004.823971 (2004).
13. Fan, K. et al. Wideband horizontally polarized omnidirectional antenna with a conical beam for millimeter-wave applications. *IEEE Trans. Antennas Propag.* **66**(9), 4437–4448. https://doi.org/10.1109/TAP.2018.2851363 (2018).
14. Hu, J., Li, Y., Wang, S. & Zhang, Z. Millimeter-wave air-filled slot antenna with conical beam based on bulk silicon MEMS technology. *IEEE Trans. Antennas Propag.* **68**(5), 4077–4081. https://doi.org/10.1109/TAP.2019.2949421 (2019).
15. Yang, J., Qi, S. S., Wu, W. & Fang, D. G. A novel high-gain sum and difference conical beam-scanning reflector antenna. *IEEE Access* **8**, 103291–103300. https://doi.org/10.1109/ACCESS.2020.2998835 (2020).
16. Sanchez-Olivares, P., Masa-Campos, J. L., Garcia-Marin, E. & Escalona-Moreno, D. High-gain conical-beam traveling-wave array antenna based on a slotted circular waveguide at Ku-band. *IEEE Trans. Antennas Propag.* **68**(8), 6435–6440. https://doi.org/10.1109/TAP.2020.2970031 (2020).
17. Pham, D. A., Lee, M. & Lim, S. High-gain conical-beam planar antenna for millimeter-wave drone applications. *IEEE Trans. Antennas Propag.* **69**(10), 6959–6964. https://doi.org/10.1109/TAP.2021.3070662 (2021).
18. Row, J. S. & Lin, T. Y. Frequency-reconfigurable coplanar patch antenna with conical radiation. *IEEE Antennas Wirel. Propag. Lett.* **9**, 1088–1091. https://doi.org/10.1109/LAWP.2010.2093118 (2010).
19. Yang, J., Qi, S. S., Yu, Y. H., Wu, W. & Fang, D. G. A transmitarray illuminated by a pencil beam source to obtain conical beam with fixed linear polarization and circular polarization. *IEEE Trans. Antennas Propag.* **70**(6), 4878–4883. https://doi.org/10.1109/TAP.2021.3138490 (2022).
20. Qi, S. S., Wu, W. & Fang, D. G. Singly-fed circularly polarized circular aperture antenna with conical beam. *IEEE Trans. Antennas Propag.* **61**, 3345–3349. https://doi.org/10.1109/TAP.2013.2253302 (2013).
21. Qi, S. S., Wu, W. & Fang, D. G. Dual/single band conical-beam nested horn antennas with dual/single pointing angles. *IEEE Trans. Antennas Propag.* **60**(10), 4911–4915. https://doi.org/10.1109/TAP.2012.2207342 (2012).
22. Sanchez-Olivares, P., Masa-Campos, J. L. & Garcia-Marin, E. Dual-polarization and dual-band conical-beam array antenna based on dual-mode cross-slotted cylindrical waveguide. *IEEE Access* **9**, 94109–94121. https://doi.org/10.1109/ACCESS.2021.3093204 (2021).
23. Li, J. et al. SLA printed dual-band conical-beam filtering antenna. *IEEE Antennas Wirel. Propag. Lett.* **22**(10), 2462–2466. https://doi.org/10.1109/LAWP.2023.3291386 (2023).
24. Dong, Y. & Itoh, T. Metamaterial-based antennas. *Proc. IEEE* **100**, 2271–2285. https://doi.org/10.1109/JPROC.2012.2187631 (2012).
25. Kumar, P., Ali, T. & Pai, M. M. M. Electromagnetic metamaterials: A new paradigm of antenna design. *IEEE Access* **9**, 18722–18751. https://doi.org/10.1109/ACCESS.2021.3053100 (2021).
26. Li, M., Luk, K. M., Ge, L. & Zhang, K. Miniaturization of magnetoelectric dipole antenna by using metamaterial loading. *IEEE Trans. Antennas Propag.* **64**, 4914–4918. https://doi.org/10.1109/TAP.2016.2599176 (2016).
27. Rajanna, P. K. T., Rudramuni, K. & Kandasamy, K. A high-gain circularly polarized antenna using zero-index metamaterial. *IEEE Antennas Wirel. Propag. Lett.* **18**, 1129–1133. https://doi.org/10.1109/LAWP.2019.2910805 (2019).
28. Li, Y. & Chen, J. Design of miniaturized high gain bow-tie antenna. *IEEE Trans. Antennas Propag.* **70**, 738–743. https://doi.org/10.1109/TAP.2021.3098595 (2022).
29. Chen, Q., Zhang, H., Shao, Y. J. & Zhong, T. Bandwidth and gain improvement of an L-shaped slot antenna with metamaterial loading. *IEEE Antennas Wirel. Propag. Lett.* **17**, 1411–1415. https://doi.org/10.1109/LAWP.2018.2848639 (2018).
30. Liu, Y. & Zhao, X. Perfect absorber metamaterial for designing low-RCS patch antenna. *IEEE Antennas Wirel. Propag. Lett.* **13**, 1473–1476. https://doi.org/10.1109/LAWP.2014.2341299 (2014).
31. Khan, I., Zhang, K., Ali, L. & Wu, Q. Enhanced quad-port MIMO antenna isolation with metamaterial superstrate. *IEEE Antennas Wirel. Propag. Lett.* **23**, 439–443. https://doi.org/10.1109/LAWP.2023.3328002 (2024).
32. Saghanezhad, S. A. H. & Atlasbaf, Z. Miniaturized dual-band CPW-fed antennas loaded with u-shaped metamaterials. *IEEE Antennas Wirel. Propag. Lett.* **14**, 658–661. https://doi.org/10.1109/LAWP.2014.2376554 (2015).
33. Duan, Z., Hummelt, J. S., Shapiro, M. A. & Temkin, R. J. Sub-wavelength waveguide loaded by a complementary electric metamaterial for vacuum electron devices. *Phys. Plasmas.* https://doi.org/10.1063/1.4897392 (2014).
34. Pozar, D. M. *Microwave Engineering* 3rd edn. (Wiley, 2005).
35. Ansys HFSS. Accessed: Sep. 12, 2022. [Online]. Available: http://www.ansys.com/Products
36. Marqués, R., Martel, J., Mesa, F. & Medina, F. Left-handed-media simulation and transmission of EM waves in subwavelength split-ring-resonator-loaded metallic waveguides. *Phys. Rev. Lett.* **89**(18), 183901. https://doi.org/10.1103/PhysRevLett.89.183901 (2002).
37. Xu, H. et al. Effective-medium models and experiments for extraordinary transmission in metamaterial-loaded waveguides. *Appl. Phys. Lett.* **92**(4), 041122. https://doi.org/10.1063/1.2840163 (2008).
38. Tang, X. et al. Dual band metamaterial Cherenkov oscillator with a waveguide coupler. *IEEE Trans. Electron Devices* **64**(5), 2376–2382. https://doi.org/10.1109/TED.2017.2681074 (2017).
39. Wang, X. et al. Characterization of metamaterial slow-wave structure loaded with complementary electric split-ring resonators. *IEEE Trans. Microw. Theory Techn.* **67**(6), 2238–2246. https://doi.org/10.1109/TMTT.2019.2908360 (2019).
40. Tang, X. et al. Metamaterial-inspired backward wave oscillator using a dual band coaxial coupler. *IEEE Electron Device Lett.* **44**(9), 1559–1562. https://doi.org/10.1109/LED.2023.3294759 (2023).
41. CST Microwave Studio. CST Computer Simulation Technology, Darmstadt, Germany. Accessed: Oct. 12, 2022. [Online]. Available: http://www.cst.com
42. Li, Y., Zhao, Z., Tang, Z. & Yin, Y. Differentially fed dual-band dual-polarized filtering antenna with high selectivity for 5G sub-6 GHz base station applications. *IEEE Trans. Antennas Propag.* **68**(4), 3231–3236. https://doi.org/10.1109/TAP.2019.2957720 (2020).

Acknowledgements
This work was supported by National Natural Science Foundation of China (No. 62301459), Fundamental Research Funds for the Central Universities (No. 2682023CX076), and Natural Science Foundation of Sichuan, China (No. 2024NSFSC1432).

Author contributions
Xianfeng Tang prepared the entire text section and all computational data. Junli Lu participated the antenna test. Che Xu participated helpful discussion. Xiangqiang Li, Che Xu, Qingfeng Wang, and Jianqiong Zhang reviewed

the entire manuscript.

Competing interests
The authors declare no competing interests.

Additional information
Correspondence and requests for materials should be addressed to X.T. or C.X.

Reprints and permissions information is available at www.nature.com/reprints.

Publisher's note Springer Nature remains neutral with regard to jurisdictional claims in published maps and institutional affiliations.